NASA Contractor Report 3970

# Design of Fuselage Shapes for Natural Laminar Flow

S. S. Dodbele and C. P. van Dam
*Vigyan Research Associates, Inc.*
*Hampton, Virginia*

P. M. H. W. Vijgen
*Univeristy of Kansas*
*Lawrence, Kansas*

Prepared for
Langley Research Center
under Contract NAS1-17926

NASA
National Aeronautics
and Space Administration

**Scientific and Technical**
**Information Branch**

1986

## Table of Contents

## Abstract

Recent technological advances in airplane construction techniques and materials employing bonded and milled aluminum skins and composite materials allow for the production of aerodynamic surfaces without significant waviness and roughness, permitting long runs of natural laminar flow (NLF). These advances lead to excellent opportunities for reducing the drag of aircraft by increasing the extent of NLF. The present research effort seeks to refine and validate computational design tools for use in the design of axisymmetric and nonaxisymmetric natural-laminar-flow bodies. The principal tasks of the investigation involve fuselage body shaping using a computational design procedure.

Under Phase I SBIR funding for this research, analytical methods were refined and exploratory calculations were conducted to predict laminar boundary-layer behavior on selected body shapes. Using a low-order surface-singularity aerodynamic analysis program pressure distribution, boundary-layer development, transition location and drag coefficient have been obtained for a number of body shapes including a representative business-aircraft fuselage. Extensive runs of laminar flow were predicted in regions of favorable pressure gradient on smooth body surfaces. A computational design procedure was developed to obtain a body shape with minimum drag coefficient having large extent of NLF. Some preliminary results from the design efforts have been obtained and further work is underway.

The proposed study has widespread commercial applications. A significant reduction in the drag produced by any airplane can be obtained when extensive runs of natural laminar flow are achieved on its fuselage resulting in improved airplane performance and efficiency.

## Nomenclature

| | |
|---|---|
| $C_D$ | Drag coefficient |
| $C_P$ | Pressure coefficient |
| D | Maximum diameter |
| $f_r$ | Fineness ratio, length/maximum diameter |
| H | Boundary-layer shape factor, $\delta^*/\theta$ |
| $k_1$ | Nondimensional curvature at $x_m$ |
| L | Body length |
| M | Mach number |
| NLF | Natural Laminar Flow |
| n | Logarithmic exponent of T-S wave growth ratio |
| $R_i$ | Profile radius at $x_i$ |
| $R_n$ | Radius of curvature at the nose |
| $R_L$ | Reynolds number based on free-stream conditions and body length |
| $R_s$ | Reynolds number based on local conditions and surface length |
| $R_x$ | Reynolds number based on local conditions and axial length |
| $R_V$ | Body volume Reynolds number based on free-stream conditions and $V^{1/3}$ |
| $R_\theta$ | Reynolds number based on local conditions and boundary-layer momentum thickness |
| $r_i$ | Nondimensional profile radius of $x_i$, $2f_rR_i/L$ |
| $r_n$ | Nondimensional radius of curvature at the nose, $4x_mf_rR_n/L$ |
| $r_\infty$ | Nondimensional profile radius at x |
| $S_i$ | Profile slope at $x_i$ |
| s | Surface length, starting at the nose |
| $s_i$ | Nondimensional profile slope at $x_i$, $\frac{-2f_r(X_i-X_m)\ S_i}{(L-r_i)}$ |

| | |
|---|---|
| $U_\infty$ | Free-stream velocity |
| $v$ | Local velocity |
| $V$ | Body volume |
| $x$ | Axial coordinate, starting at the nose |
| $X_i$ | Axial location of inflection point |
| $X_m$ | Axial location of maximum diameter |
| $x_m$ | Nondimensional axial location of maximum diameter, $X_m/L$ |
| $x_i$ | Nondimensional axial location of inflection point, $X_i/L$ |
| $x_{sep}$ | Nondimensional axial length coordinate of boundary-layer separation |
| $x$ | Nondimensional axial location, X/L |
| $Z(x)$ | Nondimensional thickness distribution |
| $\alpha$ | Angle of attack (degrees) |
| $\delta^*$ | Boundary-layer displacement thickness |
| $\theta$ | Boundary-layer momentum thickness |
| $\phi$ | Half trailing-edge angle at the tail (see fig. 15) in degrees |

## 1. Introduction

In recent years, airplane construction material and fabrication methods have improved greatly, resulting in the production of airframe surfaces which accurately match the design shape. Recent flight tests (refs. 1 and 2) have demonstrated that extensive runs of laminar boundary layer flow can be obtained over regions of favorable pressure gradient on smooth airplane surfaces and provide a significant reduction in profile drag. A major portion of the past research effort for achieving and maintaining natural laminar flow (NLF) has been focused on aircraft wings. Fuselage shaping to increase the extent of NLF has received much less attention in the literature except for sailplane bodies and hydrodynamic bodies.

Althaus (ref. 3) conducted experimental investigations in order to show the possible reduction in drag of sailplane fuselages and study the flow interaction of the fuselage with a wing and the influence of various wing positions. In reference 4 an analytical and experimental study on NLF nacelles demonstrates the presence of significant regions of laminar flow on the surface of a turbofan engine nacelle. Sub-scale wind-tunnel testing of the NLF nacelle indicated a potential of 1.5-2.0 percent reduction in total airplane drag by maintaining laminar boundary-layer flow over extensive regions of the external nacelle surface. The pay-off in terms of airplane profile drag reduction can be much larger when considering the application of low-drag NLF design to airplane fuselages. The importance of fuselage skin-friction drag is clearly indicated in figure 1, in which a profile drag breakdown is shown for a typical transport jet (ref. 5). The fuselage generates less than 50 percent of the profile drag for the all-turbulent airplane. However, it is estimated that the contribution of the fuselage to airplane profile drag increases to more than 70 percent of

the total profile drag if extensive regions of natural laminar flow are achieved on the wing and tail surfaces. The present study will investigate the design of fuselage shapes that result in extensive regions of NLF at conditions corresponding to typical cruise Reynolds numbers encountered by touring, business and transport airplanes.

Carmichael (ref. 6) did an experimental study on a body of fineness ratio of 3.33 developed by revolving the coordinates of a NACA-66 laminar flow airfoil about the longitudinal axis. This tailboomed body (called the Dolphin) was tested over a Reynolds number range of 20 million to 30 million (based on body length) and transition length Reynolds numbers of 14 million to 18 million were obtained. Boundary-layer transition from laminar to turbulent flow apparently occured beyond the point of maximum thickness. These results indicate that a low fineness ratio and a proper shape can produce a strong favorable pressure graident (and therefore a strong flow acceleration) on the forebody of the configuration. As a result the boundary layer stays laminar over an appreciable distance.

Dalton and Zedan (ref. 7) presented an inverse method to design low-drag axisymmetric body shapes. A prescribed surface-velocity distribution is input and the corresponding body shape is computed. The method is based on representing the body of revolution by a source distribution of variable intensity along its axis. Dalton and Zedan applied the method to carry out a design study for bodies at a volume Reynolds number $R_V$ = 50 million. This Reynolds number is representative for large torpedo and small airship applications and it corresponds to a length Reynolds number $R_L$ of approximately 200 million depending on body shape.

Forebody shapes of missiles designed specifically for long runs of NLF at compressible free-stream velocities have been studied in reference 8. In

reference 8, results computed for three forebody shapes of different fineness ratios (1.0, 1.5 and 2.0) indicate that laminar flow can be obtained for high Reynolds numbers and high subsonic Mach numbers. The design condition for these relatively blunt forebody shapes was a unit Reynolds number of 40 million per foot and a Mach number of 0.75. However, the Reynolds number range which is encountered by most airplanes is in the range of 1-3 million per foot. Therefore, the results of reference 8 are not very useful for the design of fuselage forebodies for subsonic airplanes.

Parsons and his coworkers (refs. 9 and 10) have given a procedure to design axisymmetric bodies for minimum drag for hydrodynamic applications. Drag reduction is accomplished solely through manipulation of the vehicle shape. The optimization problem is formulated as a nongradient search in a finite constrained parameter space. Two classes of bodies, described by five and eight parameters, are considered. The requirement for nonseparating flow represents an additional constraint on the optimization problem. The axisymmetric bodies are represented by axial singularity distribution and the drag coefficient is evaluated using Young's formula. The results show that significant drag reduction is possible through shape manipulation. Pinebrook (refs. 11 and 12) devised a technique, based on an evolution strategy, to minimize the drag of an axisymmetric body with a given maximum body diameter and fineness ratio. The body profile is described by continuous first order axial singularity distribution defined at 21 points. The gradual body profile changes are effected through a process derived from the evolution strategy. The drag is calculated from the momentum deficit in the boundary layer at the end of the body using Young's formula (ref. 13). The bodies designed by Pinebrook had laminar flow only up to 3 percent of the body length from the nose

at which location the boundary layer was tripped.

According to von Karman (ref. 14) not every axisymmetric body can be represented accurately by an axial source distribution. Also, recently Hess (ref. 15) pointed out that the line sources cannot extend to the ends of the body at finite strengths otherwise the velocities there will be infinite. These problems with the axial singularities are eliminated if one uses panel methods with which the body is represented by aerodynamic surface panels. Here, a computational procedure was developed to obtain fuselage geometries for considerable extent of laminar flow and hence for low skin-friction drag.

## Computational Design Procedure

The computational design procedure used to obtain "natural laminar flow fuselage" geometries is described in the flow chart (see fig. 2). Initial values of the design variables describing the body shape are input along with the Reynolds number (based on length), the nondimensional length and the fineness ratio. The axisymmetric body is described by seven parameters. The expressions to obtain the body shape are given in the Appendix.

A number of constraints are imposed on the design parameters in order to generate designs which are realistic and practical. The geometric constraints are given below.

1. $0 \leq r_n$
2. $0 \leq k_1$
3. $0 < x_m < x_i < 1$
4. $0 \leq r_i \leq 1$
5. $0 \leq s_i$
6. $5° \leq \phi \leq 80°$
7. No inflection on forebody, midbody and afterbody except at $x_i$.

These conditions are taken care of by choosing proper upper and lower bounds for the design variables.

The other constraint is that the separation takes place very near the trailing edge. The following constraint is imposed in the optimization procedure:

$$0.95 \leq x_{sep}$$

The objective function is taken to be body profile drag coefficient which is obtained by Young's formula (ref. 13). This objective function is to be minimized subjected to the constraints which are given above. The optimizer computes the gradients of the objective function and then, using either a conjugate direction method or a method of feasible direction, determines a linear search direction, along which a new constrained variable is constructed.

An improved or minimum feasible objective functional value is evaluated and a series of proposed updated design variables are calculated. The objective function and the constrained function are evaluated using the updated design variables, interpolating over the range of feasible proposed design variables resulting in a minimum value of the objective function. The results are tested against a convergence criteria. The procedure will stop if the convergence criteria is satisfied giving a body shape with minimum drag or maximum transition length satisfying the separation constraint. If the convergence criteria is not satisfied the design parameters go through the analyzer again resulting in a new set of design variables and the procedure is repeated until a final shape is obtained. The method involves a constrained minimization procedure (ref. 25) coupled with an aerodynamic analysis program based on a low-order surface singularity method named "VSAERO" (ref. 16). Pressure distribution and velocity distribution can be computed by the aerodynamic analysis program which uses surface singularity panels to represent the body. The program also calcu-

lates the effect of the viscous boundary layer adjacent to the body. Integral methods are used to predict the boundary-layer development. The laminar part of the boundary layer is calculated by Thwaite's method with Curle's modification. Boundary-layer transition is predicted by Granville's procedure. Nash and Hick's method is used for the turbulent boundary-layer calculations. Laminar separation/turbulent reattachment calculations are done empirically using Gaster's measurements.

## Aerodynamic Analysis

To validate the surface singularity method, inviscid pressure distributions have been obtained for the following configurations:

(a) a sailplane body,

(b) an axisymmetric body with an ogival nose, a cylindrical center body and a flared afterbody,

(c) an ellipsoid of revolution,

(d) a body of revolution with a long favorable pressure gradient,

(e) a low-drag body of revolution considered by Parsons et al. (ref. 10)

(f) a representative business aircraft fuselage, and

(g) a body of revolution whose maximum diameter and length correspond to those of the configuration (f).

In reference 3, Althaus presents wind-tunnel measurements on bodies and wing-body combinations obtained at the University of Stuttgart. The measurements include lift and drag characteristics, surface velocity distributions, and boundary-layer transition locations. Each of the bodies of revolution had a fineness ratio of 10 and a length of 6.56 ft (2.0 m) and the measurements were obtained at

a Reynolds number (based on body length) $R_L$ = 7.1 million. Althaus' body shape 2 was modeled by surface singularity panels to obtain velocity distributions. In figure 3, the theoretical velocity distributions are compared with surface velocity measurements. In the figure, the body shape is also shown for this fuselage model. In the pressure recovery region theoretical results do not agree very well with the wind-tunnel data. Also, at X/L = 0.12 a kink appears in the calculated velocity distribution. This disturbance is produced when the body coordinates as given by Althaus in reference 3 are used to model the body shape. Consequently, the prediction of the boundary-layer transition location does not agree very well with the experimental result. In the tunnel, transition was measured at X/L = 0.36 at $R_L$ = 7.1 million. The Granville criterion predicted transition location at X/L = 0.29 which is slightly forward compared to the experimental result. This can be expected because of the velocity discrepancies in the pressure-recovery region. These discrepancies appear to be caused by wind-tunnel blockage effects, which produce higher surface velocities near the location of maximum body diameter.

Very good agreement between measured and calculated surface pressure coefficients was obtained for a body of revolution (configuration b) tested by Fox in the NASA Langley high-speed 7- by 10-foot wind tunnel (ref. 17). In figure 4, the results are shown for Fox's configuration 5, an axisymmetric body composed of an ogival nose, a cylindrical centerbody and a flared afterbody. Surface pressure data are plotted as function of the orifice location for the orifices on the longitudinal meridian. By using the surface singularity method, the pressure coefficients are obtained and they are also presented in figure 4. The method allows modeling of the wake which originates from the edge of the blunt base. However, for simplicity when the blunt base and the sting were replaced with a 10-degree cone (the flared afterbody has an identical

slope of 10 degrees) the comparison of theoretical results with experimental data showed very good agreement.

Measurements of pressure and boundary-layer transition were made on the ellipsoid of revolution (configuration c) in wind tunnels and boundary-layer transition was also measured in flight (ref. 18). Figure 5 presents the surface pressure distribution and transition location for the ellipsoid of revolution of fineness ratio 9. The viscous calculations were done at $R_L$ = 13.98 million. As shown in the figure, although the pressure distributions compare well, the computed transition location does not agree very well with the experimental data. The transition length Reynolds number was 5.08 million. Granville's boundary-layer transition criterion, which is used in the present computation, predicts transition further downstream than was measured in the experiment (ref. 18). The same behavior occured when the Reynolds number was increased to 22.03 million. Kaups (ref. 19) also computed transition location for this ellipsoid by using Granville's criterion and also arrived at the fact that at these two Reynolds numbers, transition is predicted at points further downstream than at the locations observed in the experiments (in flight and wind tunnel). Kaups concluded that none of the transition prediction methods (including the $e^9$-method of Smith and Gamberoni) gave consistent satisfactory answers for the ellipsoid. It appears that for bodies with flat pressure distributions considerable amount of uncertainty exists in the computation of transition location.†

Next, a low-drag body of revolution with fineness ratio 4.5, with a long favorable pressure gradient forebody (configuration d) was analyzed. Hansen and Hoyt (ref. 20) studied this body experimentally and measured drag and intermittency and calculated the surface-pressure distribution. In figure

†In private communication, Dr. Pfenninger has indicated that the F94 boundary-layer transition data appears to be adversely affected by excessive engine sound levels.

6, comparison is made between Hansen and Hoyt's results and the predictions obtained by the present method. In the present computations transition is predicted at X/L = 0.67 due to laminar separation for $R_L$ = 10.86 million. Hansen and Hoyt predicted transition at X/L = 0.68.

Another low-drag body called X-35 (configuration e) studied by Parsons et al. (ref. 10) was also analyzed. The predicted surface-velocity distribution agrees very well with that presented in reference 10 (see fig. 7). Parsons uses the Michel-$e^9$ correlation to predict boundary-layer transition. The Michel-$e^9$ correlation provides a relation between $R_\theta$ and $R_s$ at transition (ref. 21):

$$R_\theta = 1.174\ (1 + 22400/R_s)R_s^{0.46} \tag{1}$$

The results in figure 8 indicate that no catastrophic Tollmien-Schlichting growth is predicted and transition due to laminar separation occurs at X/L = 0.68. Granville's transition criterion is more conservative for the X-35 body with transition predicted at X/L = 0.35 for $R_L$ = 37.14 million. This discrepancy in the prediction of transition location has been further analyzed by applying the H-$R_x$ boundary-layer transition criterion by Wazzan, Gazley and Smith (ref. 22) and also by performing a linear stability analysis of the laminar boundary layer. The H-$R_x$ method correlates the boundary-layer shape factor $H = \delta^*/\theta$ and $R_s$ at transition as follows:

$$\log[R_s(e^9)] = -40.4557 + 64.8066\ H - 26.7538\ H^2 + 3.3819\ H^3 \quad \text{for } 2.1 < H < 2.8 \tag{2}$$

The results in figure 9 show that according to this method boundary-layer transition occurs at X/L = 0.25. The linear stability analysis of the laminar boundary layer has been performed using the SALLY code (ref. 23). Input to this

program is provided by a modified version of the Harris finite-difference boundary-layer code (ref. 24). In figure 10, the logarithmic disturbance amplitude ratio or "n-factor" is plotted as a function of the nondimensional axial distance X/L for a range of Tollmien-Schlichting disturbance frequencies. The envelope of these curves shows that an n-factor of 9 is reached at X/L = 0.185, while at X/L = 0.25 the n-factor is about 12.5. In summary, it appears that the Michel-$e^9$ criterion as used by Parsons et al. (ref. 10) provides transition results which are too optimistic.

Next, a representative business aircraft fuselage of fineness ratio about 6 (configuration f) was analyzed. Inviscid pressure distributions on the upper and the lower surface were calculated and are presented in figure 11. Laminar-turbulent transition prediction was made using Granville's criterion at a unit Reynolds number of 1 million per foot ($R_L$ = 40.86 million) and it is indicated in the figure (transition Reynolds number range is 4.1 million - 16.0 million). It is to be noted that it is not possible to analyze these kinds of practical nonaxisymmetric bodies by using axial singularity distributions. Furthermore, the transition prediction assumed no three-dimensional boundary-layer stability effects. While this assumption might limit the validity of the present transition prediction, the value of that limit (say in terms of Reynolds number) is not known. The validity of this prediction remains to be checked with experimental data.

Finally a body of revolution whose maximum diameter and length (configuration g) correspond to those of the representative business aircraft fuselage configuration (configuration f) is considered. Also this configuration can be thought of as a special case obtained by setting the longitudinal camber equal to zero in the more generalized configuration given by configuration f. Predicted inviscid pressure distributions and transition location are presented in figure 12 for zero angle of attack.

## Results from the Design Procedure

Preliminary results obtained by the optimization procedure are discussed through an example and are given in Table 1. The analysis is for an angle of attack of zero and the flow is assumed to be incompressible. Initially the axisymmetric body is modeled by a set of initial values of the design parameters. The fineness ratio is fixed at 6.14 and the design Reynolds number (based on length) $R_L$ is 40.86 million. The upper and the lower bounds of the design variables are also input. In the present calculation profile drag coefficient is chosen as the objective function to be minimized. The design parameters at the end of each iteration are presented in Table 1 along with the objective function. For the above example the design procedure converged at the end of the 8th iteration. Since the initial values of the design variables were not too far from the optimized design variables the process converged in 8 iterations. Judicious choice of the starting solution helps in achieving the final optimized solution in a lesser number of iterations. The initial body shape, given by the design parameters in the first row of Table 1, is sketched in figure 13. The pressure distribution for the body is also shown in the figure. For this initial body the transition location was computed at X/L = 0.36. The improvements in the transition location through the next few iterations along with the final converged value are indicated in Table 1. We see from Table 1 that the transition location is pushed further aft for the final body shape and accordingly the drag is reduced. The final body shape along with the pressure distribution are sketched in figure 14.

As explained earlier for computing the transition locations Granville's criterion is used in the analysis. Since to date there exists no satisfactory method to predict the transitional region on an axisymmetric body Granville's criterion has been used in the optimization cycle. Since one can predict growth of Tollmien-Schlichting waves downstream of the neutral point in the

laminar boundary layer using linear stability analysis it is logical to include it in the design process itself. But in view of the computational costs and complexities, direct incorporation of the boundary-layer stability analysis in the optimization procedure was avoided and Granville's criterion was used for predicting the transition.

## Summary

Present airplane construction techniques result in the production of smooth and accurate aerodynamic surfaces over which long runs of natural laminar boundary-layer flow (NLF) can be obtained. A major portion of the past research effort for achieving NLF has been focused on airplane lifting surfaces. However, fuselage shaping to achieve considerable regions of NLF has received limited attention. Recent introduction of business and commuter airplanes with low-drag NLF lifting surfaces justifies study of the feasibility of NLF over fuselage surfaces and thereby providing possibilities to decrease airplane profile drag.

In Phase I of the research effort, a low-order surface-singularity analysis was used to obtain surface-pressure distribution over a selected number of body shapes, including a representative nonaxisymmetric business-aircraft fuselage. Using an integral boundary-layer method, predictions of transition location and drag coefficient have been obtained for these body shapes. Extensive runs of NLF are predicted over regions of favorable pressure gradient on smooth surfaces of both axisymmetric and nonaxisymmetric bodies at low angles of attack. A computational design procedure coupled with an aerodynamic analysis program was developed to obtain a body shape with large extents of NLF and minimum drag.

Comparisons of boundary-layer transition location predictions with limited

available experimental results for several bodies show poor correlation between calculated and measured transition locations. Therefore, it is proposed to use linear boundary-layer stability theory in the analysis and design of axisymmetric bodies with favorable pressure gradients for considerable runs of NLF. Presently, analytical tools are not available to calculate three-dimensional boundary-layer velocity profiles and transition location accurately under nonaxisymmetric flow conditions. Also, very limited high quality boundary-layer data under axisymmetric and nonaxisymmetric flow conditions are available at high Reynolds numbers to validate future developments in boundary-layer (stability) theory.

Based upon the results of Phase I it is recommended that a large-scale high-Reynolds-number wind-tunnel experiment be conducted to obtain high-quality boundary-layer velocity and transition data on bodies of revolution at various angles of attack. The wind-tunnel experiment which would be designed using the optimization method developed in Phase I and linear boundary-layer stability theory, would provide needed experimental data for theory validation and also demonstrate the achievability of extensive runs of NLF on commuter airplane and business-jet type of fuselages.

## References


1. Runyan, L. James; Navran, Brent H.; and Rozendaal, Rodger A.: F-111 Natural Laminar Flow Glove Flight Test Data Analysis and Boundary-Layer Stability Analysis. NASA CR-166051, January 1984.

2. Holmes, Bruce J.; Obara, C. J.; and Yip, L. P.: Natural Laminar Flow Experiments on Modern Airplane Surfaces. NASA TP-2256, June 1984.

3. Althaus, D.: Wind-Tunnel Measurements on Bodies and Wing-Body Combinations. In Motorless Flight Research, 1972, NASA CR-2315, November 1973.

4. Younghans, J. L.; and Lahti, D. J.: Analytical and Experimental Studies of Natural Laminar Flow Nacelles. AIAA Paper No. 84-0034, January 1984.

5. Quast, A.; and Horstmann, K. H.: Profile Design for Wings and Propellers. NASA TM-77785, November 1984.

6. Carmichael, B. H.: Underwater Drag Reduction Through Optimal Shape. In Underwater Missile Propulsion, edited by L. Greiner, Compass Publications, Inc., Arlington VA, 1966.

7. Dalton, C.; and Zedan, M. F.: Design of Low Drag Axisymmetric Shapes By the Inverse Method. Journal of Hydronautics, Vol. 15, Jan-Dec. 1981, pp. 48-54.

8. Barger, R. L.: A Theoretical Investigation of Forebody Shapes Designed for Natural Laminar Boundary-Layer Flow. NASA TP-1375, January 1979.

9. Parsons, J. S.: The Optimum Shaping of Axisymmetric Bodies for Minimum Drag in Incompressible Flow. Ph.D. Thesis, Purdue University, 1972.

10. Parsons, J. S.; Goodson, R. E.; and Goldschmied, F. R.: Shaping of Axisymmetric Bodies for Minimum Drag in Incompressible Flow. Journal of Hydronautics, Vol. 8, No. 3, July 1974, pp. 100-107.

11. Pinebrook, W. E.: Drag Minimization on a Body of Revolution. Ph.D. Thesis, University of Houston, 1982.

12. Pinebrook, W. E.; and Dalton, C.: Drag Minimization on a Body of Revolution Through Evolution. Computer Methods in Applied Mechanics and Engineering, Vol. 39, 1983, pp. 179-197.

13. Young, A. D.: The Calculation of Total and Skin Friction Drags of Bodies of Revolution at Zero Incidence. ARC R&M 1874, April 1939.

14. von Karman, Th.: Calculation of Pressure Distributions on Airship Hulls. NACA TM-574, 1930.

15. Hess, J. L.: The Unsuitability of Ellipsoids as Test Cases for Line-Source Methods. Journal of Aircraft, Vol. 22, No. 4, April 1985, pp. 364-367.

16. Maskew, B.: Prediction of Subsonic Aerodynamic Characteristics - A Case for Low-Order Panel Methods. Journal of Aircraft, Vol. 19, No. 2, Feb. 1982, pp. 157-163.

17. Fox, C. H., Jr.: Experimental Surface Pressure Distributions for a Family of Axisymmetric Bodies at Subsonic Speeds. NASA TM X-2439, December 1971.

18. Groth, E. E.: Boundary Layer Transition on Bodies of Revolution. Northrop Aircraft Company, Report No. NAI-57-1162 (Contract AF33(616)-3168), BLC-100, July 1957.

19. Kaups, K.: Transition Prediction on Bodies of Revolution. Douglas Aircraft Co., Report No. MDC J6530 (Contract No. N66001-74-C-0020), April 1974.

20. Hansen, R. J.; and Hoyt, J. G.: Laminar-to-Turbulent Transition on a Body of Revolution with an Extended Favorable Pressure Gradient Forebody. Transaction of the ASME, Vol. 106, June 1984, pp. 202-210.

21. Cebeci, T.; and Bradshaw, P: Momentum Transfer in Boundary Layers, Hemisphere Publishing Corporation, Washington, London, 1977.

22. Wazzan, A. R.; Gazley, C., Jr.; and Smith, A. M. O.: H - $R_x$ Method for Predicting Transition, AIAA Journal, Vol. 19, No. 6, June 1981, pp. 810-811.

23. Srokowski, A. J.; and Orszag, S. A.: Mass Flow Requirements for LFC Wing Design. AIAA Paper No. 77-1222, 1977.

24. Harris, J. E.; and Blanchard, D. K.: Computer Program for Solving Laminar, Transitional, or Turbulent Compressible Boundary-Layer Equations for Two-Dimensional and Axisymmetric Flow. NASA TM-83207, 1981.

25. Vanderplaats, G. N.: CONMIN: A FORTRAN Program for Constrained Function Minimization-User's Manual. NASA TM X-62282, August 1973.

## Appendix

The seven design parameters describing the body shape are taken to be:

$x_m$ = nondimensional axial location of maximum diameter D defined as $X_m/L$,

$k_1$ = nondimensional curvature at $X_m$ defined as $(-2x_m f_r)\ K_1\ L$,

$r_n$ = nondimensional radius of curvature at nose defined as $(4x_m\ f_r)R_n/L$,

$r_i$ = nondimensional profile radius at $X_i$ defined as $2f_r R_i/L$,

$s_i$ = nondimensional profile slope at $X_i$ defined as $[-2f_r(x_i - x_m)/(L - r_i)]S_i$,

$x_i$ = nondimensional axial location of inflection point defined as $X_i/L$,

$\phi$ = half trailing-edge angle of the profile,

and $X_m$, $K_1$, $R_n$, $R_i$, $S_i$ and $X_i$ are respectively the axial location of the maximum body diameter, curvature at $X_m$, radius of curvature at the nose, radius at $X_i$, slope at $X_i$ and axial location of the inflection point.

The body is devided into 3 sections each described by a low degree polynomial. The complete body profile is continuous through the second derivative to avoid local regions of highly accelerated flow. The expressions representing the forebody and the midbody are taken from reference 10. The expressions representing the afterbody were derived according to the present needs. The body has a rounded nose and a pointed conical afterbody.

The forebody ($0 \leq X \leq X_m$) is described by a fourth-degree polynomial, the midbody ($X_m \leq X \leq X_i$) by a fifth degree polynomial and the afterbody by a fourth degree polynomial. The profile has a finite slope at X = L allowing a finite trailing-edge angle. The dimensional parameters are shown in the figure 15. The analytical expressions for the nondimensional radius of the axisymmetric

body are given by

$$r(x) = \left(\frac{1}{2f_r}\right)[r_n F_1(x) + k_1 F_2(x) + G(x)]^{1/2} \quad \text{A1}$$

for $0 \leq X \leq X_m$ (forebody)

where $x = X/X_m$ A2

$$F_1(x) = -2x(x-1)^3 \quad \text{A3}$$

$$F_2(x) = -x^2(x - 1)^2 \quad \text{A4}$$

$$G(x) = x^2(3x^2 - 8x + 6) \quad \text{A5}$$

For $X_m \leq X \leq X_i$ (midbody)

$$r(x) = \left(\frac{1}{2f_r}\right) \{r_i + (1 - r_i)[k_{1_m} F_1(x) + s_i F_2(x) + G(x)]\} \quad \text{A6}$$

where $x = \left(\frac{X_i - X}{X_i - X_m}\right)$ A7

$$F_1(x) = -\frac{1}{2} x^3(x - 1)^2 \quad \text{A8}$$

$$F_2(x) = x - x^3(3x^2 - 8x + 6) \quad \text{A9}$$

$$G(x) = x^3(6x^2 - 15x + 10) \quad \text{A10}$$

$$k_{1_m} = \left[\left(\frac{x_i}{x_m}\right) - 1\right]^2 \frac{k_1}{(1 - r_i)} \quad \text{A11}$$

For $X_i \leq X \leq L$ (afterbody)

$$r(x) = s_{i_L} x(1 - x^3) - s_{i_a} x^2(2x - 3)(x - 1) + x^2(3x^2 - 8x + 6) \quad \text{A12}$$

where

$$s_{i_a} = \frac{(1 - r_i)(1 - x_i) s_i}{(x_i - x_m) r_i} \quad \text{A13}$$

$$s_{i_L} = \{\frac{2f_r\,(x_i - x_m)\,\tan\phi}{(1 - r_i)}\} \qquad \text{A14}$$

$$f_r = L/D \qquad \text{A15}$$

Table 1

Convergence of the Design Variables (SPKB1)

$f_r$ = 6.414, $R_L$ = 40.86 million, $\alpha$ = 0°

| No. of iterations | $x_m$ | $k_1$ | $r_n$ | $r_i$ | $s_i$ | $x_i$ | $\phi$ | $x_{trans}/\ell$ | $C_D$† |
|---|---|---|---|---|---|---|---|---|---|
| Initial | 0.55550 | 0.17109 | 0.35000 | 0.40000 | 2.2867 | 0.85531 | 10.011 | 0.360 | 0.0247 |
| 1 | 0.55000 | 0.17109 | 0.35000 | 0.47144 | 1.7324 | 0.85000 | 10.905 | 0.359 | 0.0237 |
| 2 | 0.55000 | 0.17109 | 0.35000 | 0.46918 | 1.6660 | 0.85260 | 10.976 | 0.359 | 0.0237 |
| 3 | 0.55491 | 0.17109 | 0.35000 | 0.46956 | 1.6660 | 0.85609 | 10.980 | 0.365 | 0.0236 |
| 4 | 0.55292 | 0.17109 | 0.35000 | 0.46949 | 1.6660 | 0.85604 | 10.984 | 0.365 | 0.0236 |
| 5 | 0.55162 | 0.17109 | 0.35000 | 0.46969 | 1.6660 | 0.85596 | 10.986 | 0.364 | 0.0235 |
| 6 | 0.55151 | 0.17109 | 0.35000 | 0.46971 | 1.6660 | 0.85595 | 10.986 | 0.359 | 0.0238 |
| 7 | 0.55145 | 0.17109 | 0.34987 | 0.46974 | 1.6660 | 0.85598 | 10.987 | 0.364 | 0.0235 |
| 8 | 0.55145 | 0.17109 | 0.34986 | 0.46974 | 1.6660 | 0.85596 | 10.987 | 0.364 | 0.0235 |

†Reference area for $C_D$ calculation was frontal area.

All- turbulent surfaces

| | |
|---|---|
| Nacelles and misc | 5.2% |
| Fuselage | 48.7% |
| Empennage | 14.3% |
| Wing | 31.8% |

| | |
|---|---|
| Nacelle and others | .0010 |
| Fuselage | .0092 |
| Empennage | .0027 |
| Wing | .0060 |
| Total profile $C_D$ | .0189 |

Laminar lifting surfaces

| | |
|---|---|
| Nacelles and misc | 7.6% |
| Fuselage | 70.2% |
| Empennage | 6.9% |
| Wing | 15.3% |

| | |
|---|---|
| Nacelle and others | .0010 |
| Fuselage | .0092 |
| Empennage | .0009 |
| Wing | .0020 |
| Total profile $C_D$ | .0131 |

Figure 1. Build-Up of Profile Drag for All-Turbulent Airbus A300 and A300 with Laminar Lifting Surfaces.

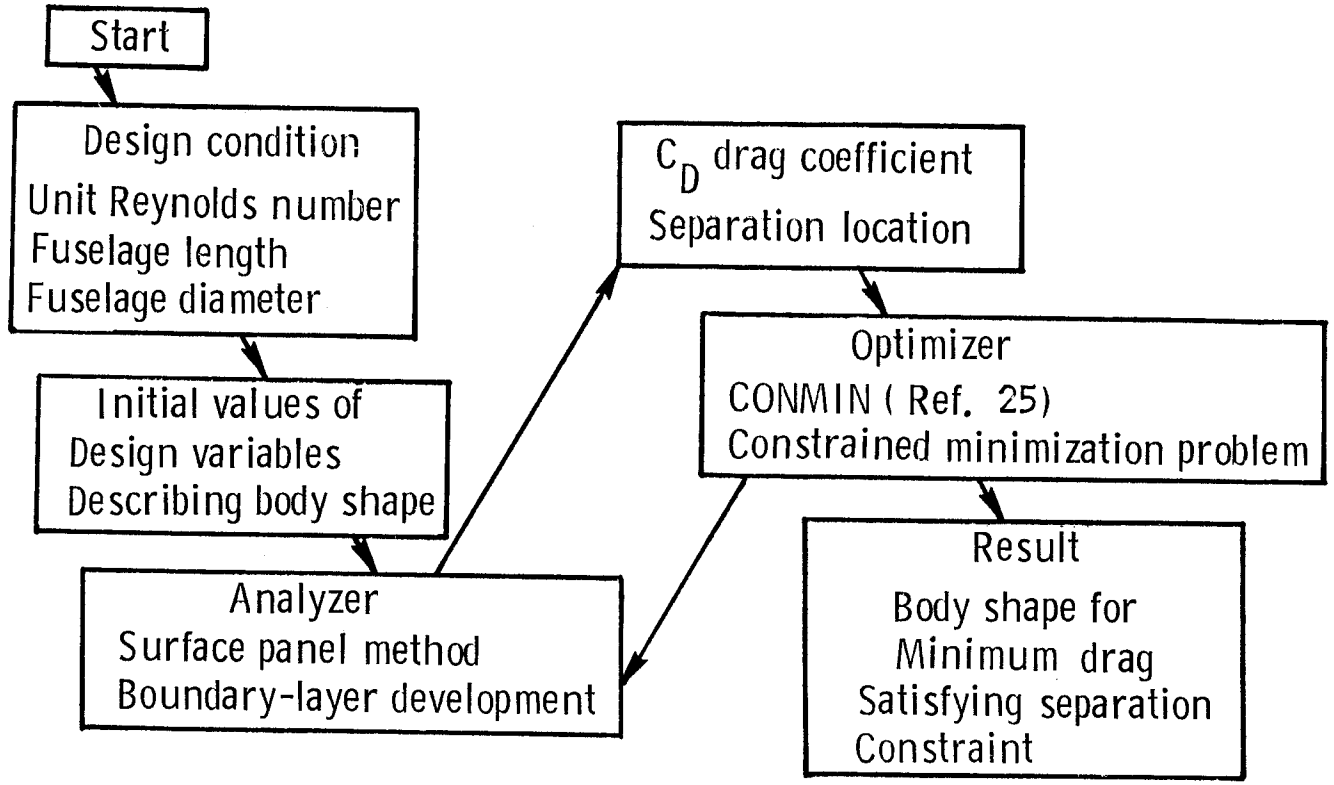


Figure 2. Flow Chart of Design Procedure for Minimum Drag Natural Laminar Flow Fuselage.

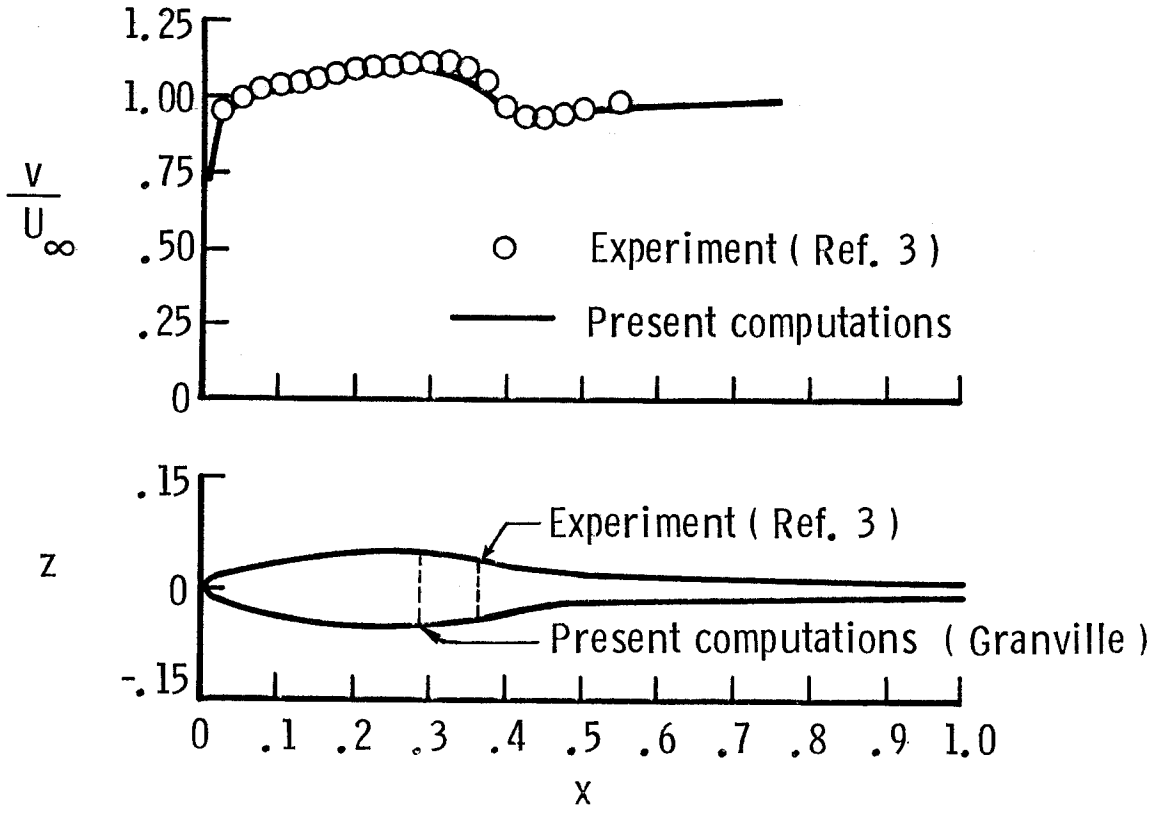


Figure 3. Velocity Distribution, Geometry and Transition Location for Fuselage Shape 2; $\alpha = 0°$, $R_L = 7.1$ million and Incompressible Flow.

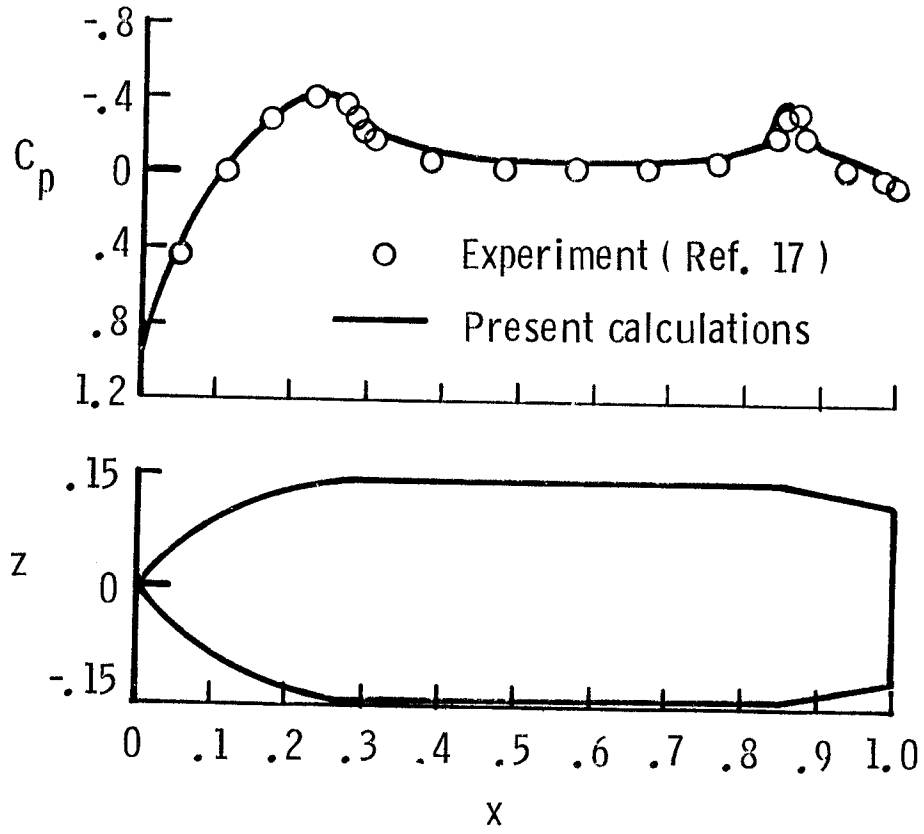


Figure 4. Surface Pressure Distribution and Geometry for Model Configuration 5 at M = 0.404 and $\alpha$ = 0.06°.

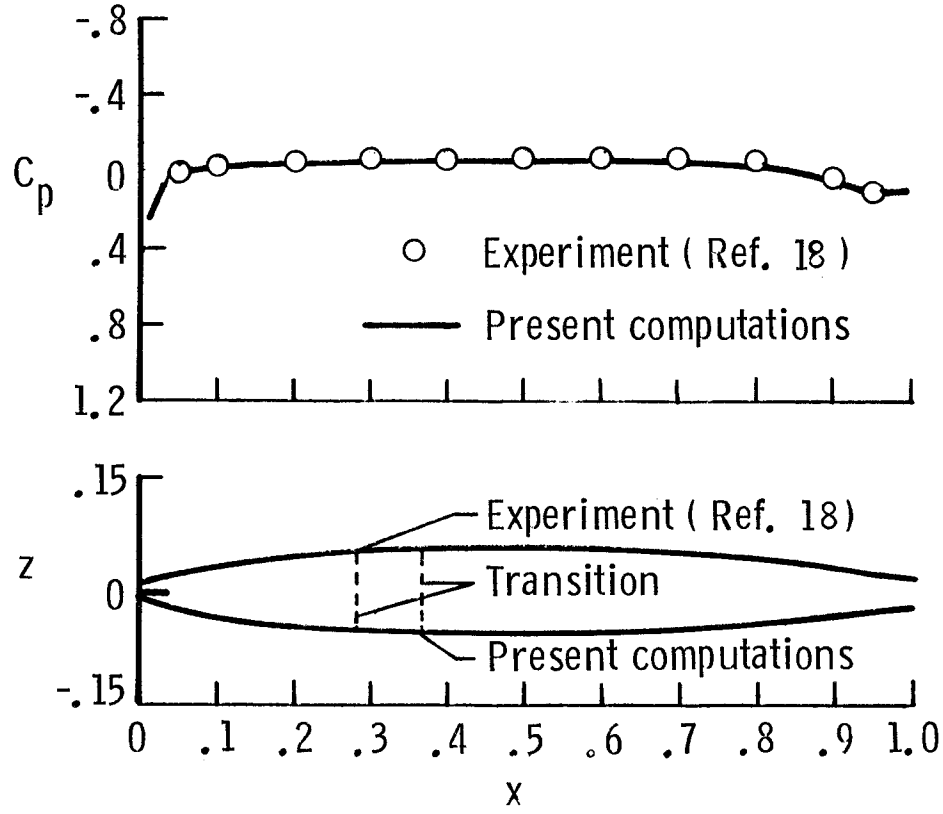


Figure 5. Surface Pressure Distribution, Geometry and Transition Location for an Ellipsoid of Revolution of Fineness Ratio 9; $\alpha = 0°$, $R_L$ = 13.98 million and Incompressible Flow.

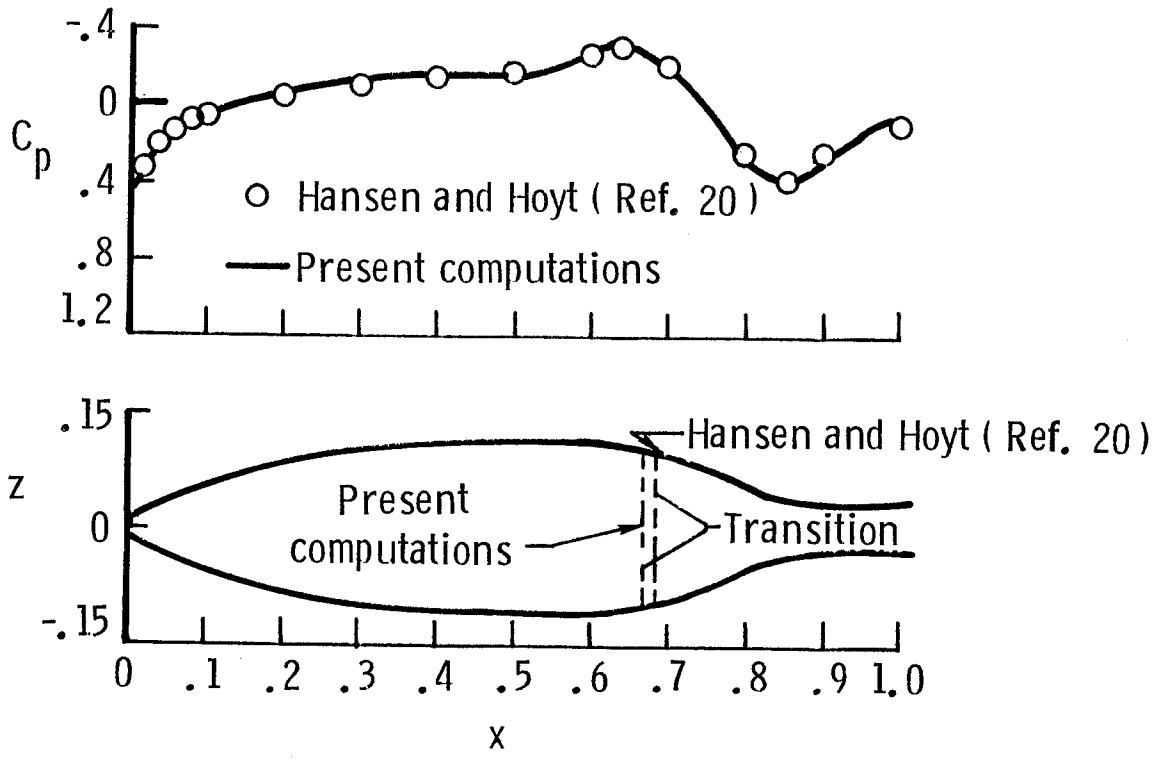


Figure 6. Pressure Distribution, Geometry and Transition Location for a Body of Revolution with Fineness Ratio 4.5; $\alpha = 0°$, $R_L = 10.48$ million and Incompressible Flow.

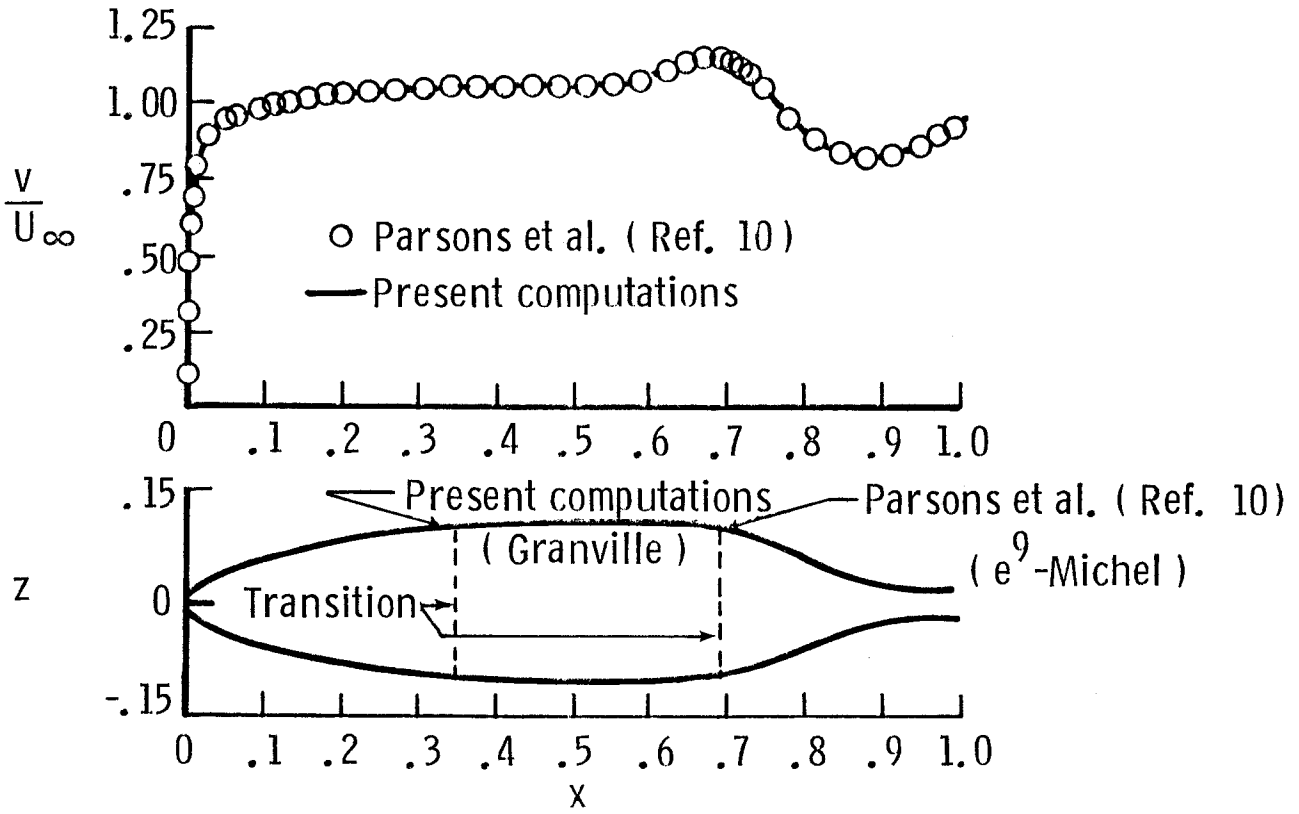


Figure 7. Surface Velocity Distribution, Geometry and Transition Location for the X-35 Body of Revolution, $\alpha = 0°$, $R_L = 37.14$ million and Incompressible Flow.

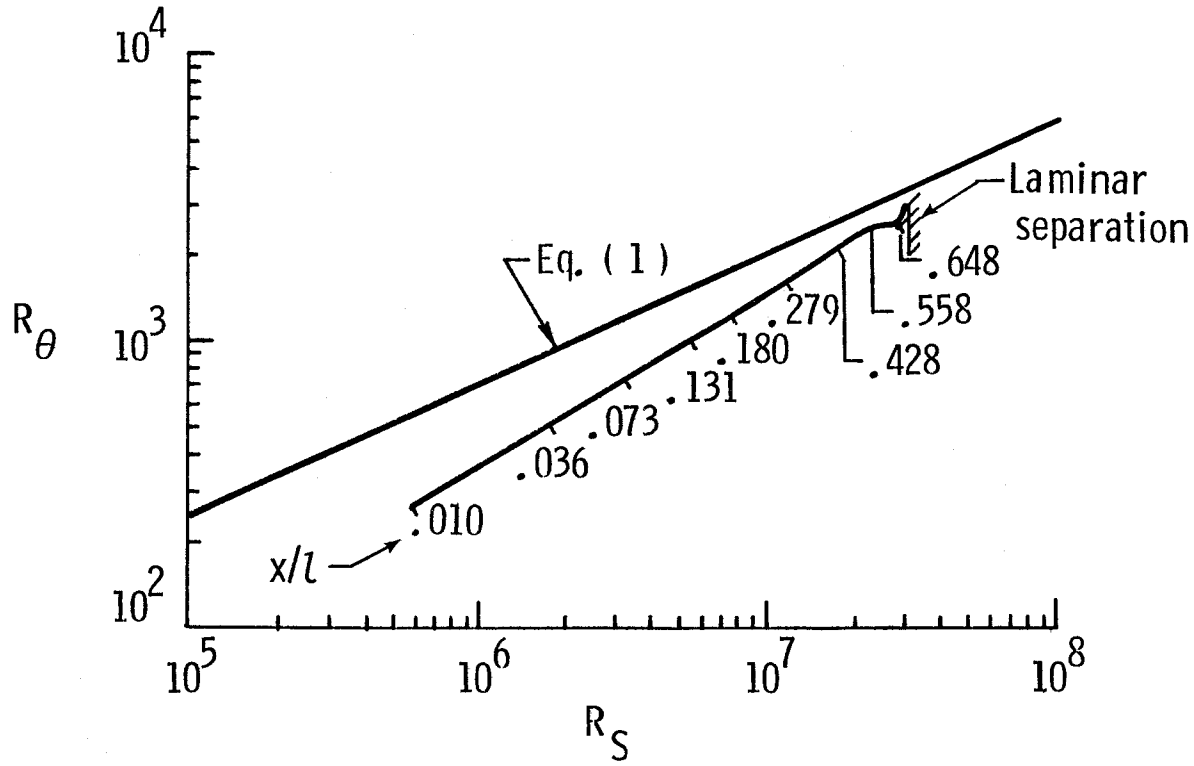


Figure 8. Boundary-Layer Development and Transition Prediction for the X-35 Body at $\alpha = 0°$, $R_L$ = 37.14 million using Michel-e[9] Correlation.

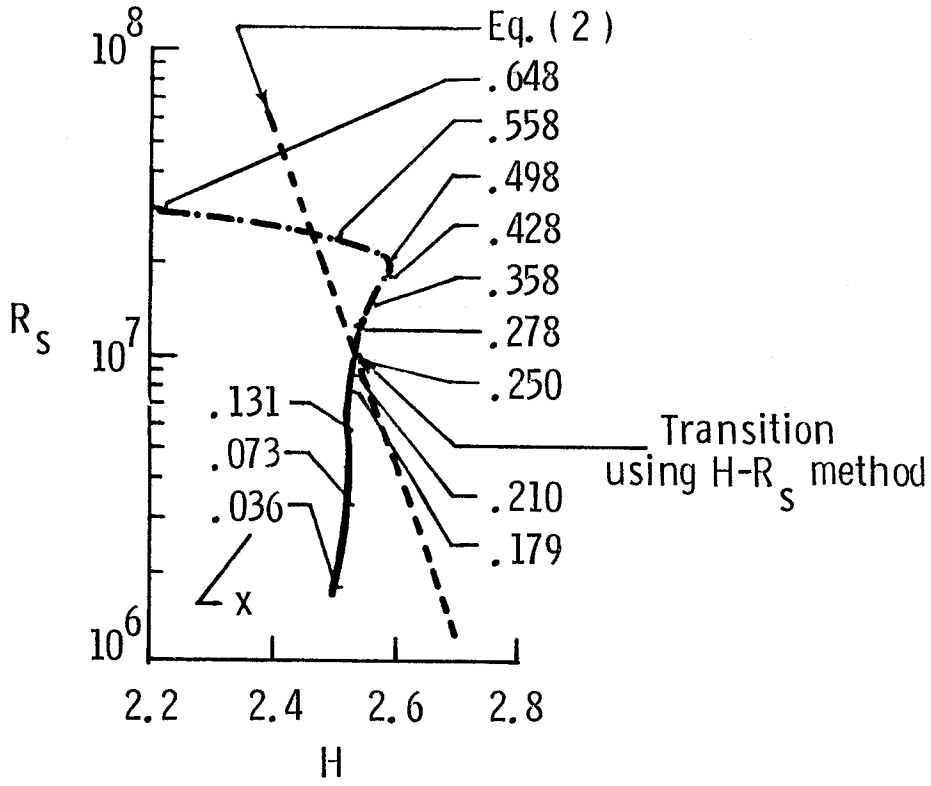


Figure 9. Boundary-Layer Development and Predicted Boundary-Layer Transition for the X-35 Body at $\alpha$ = 0°, $R_L$ = 37.14 million using H-$R_x$ Method, Incompressible Flow.

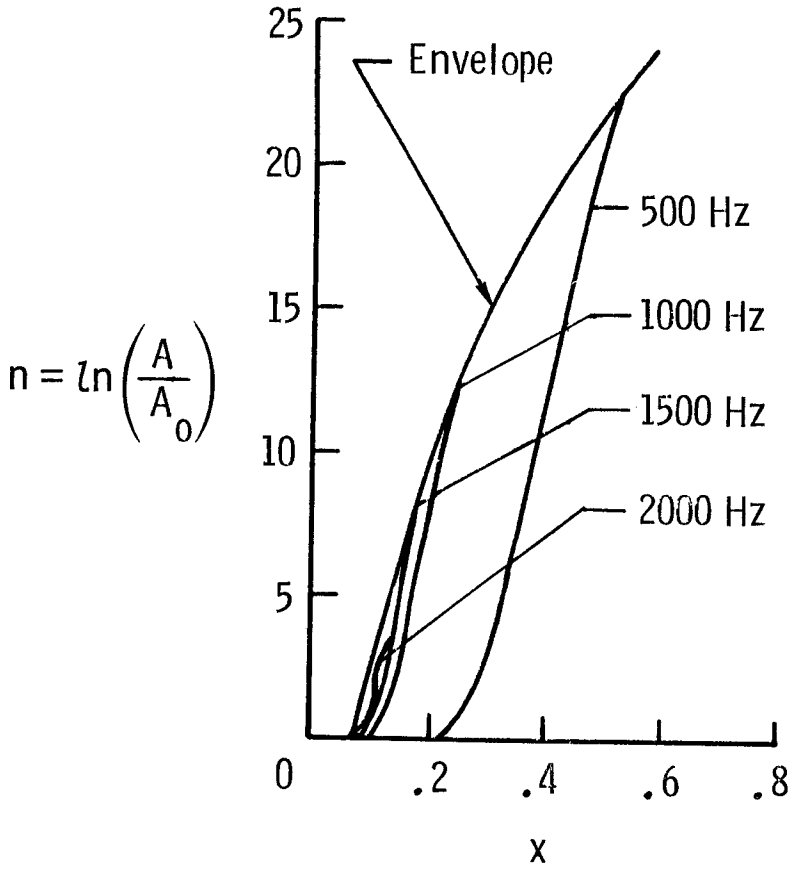


Figure 10. Logarithmic Amplification of Several Tollmien Schlichting Disturbance Frequencies for the X-35 Body of Revolution at $\alpha = 0°$, $R_L = 37.14$ million and Incompressible Flow.

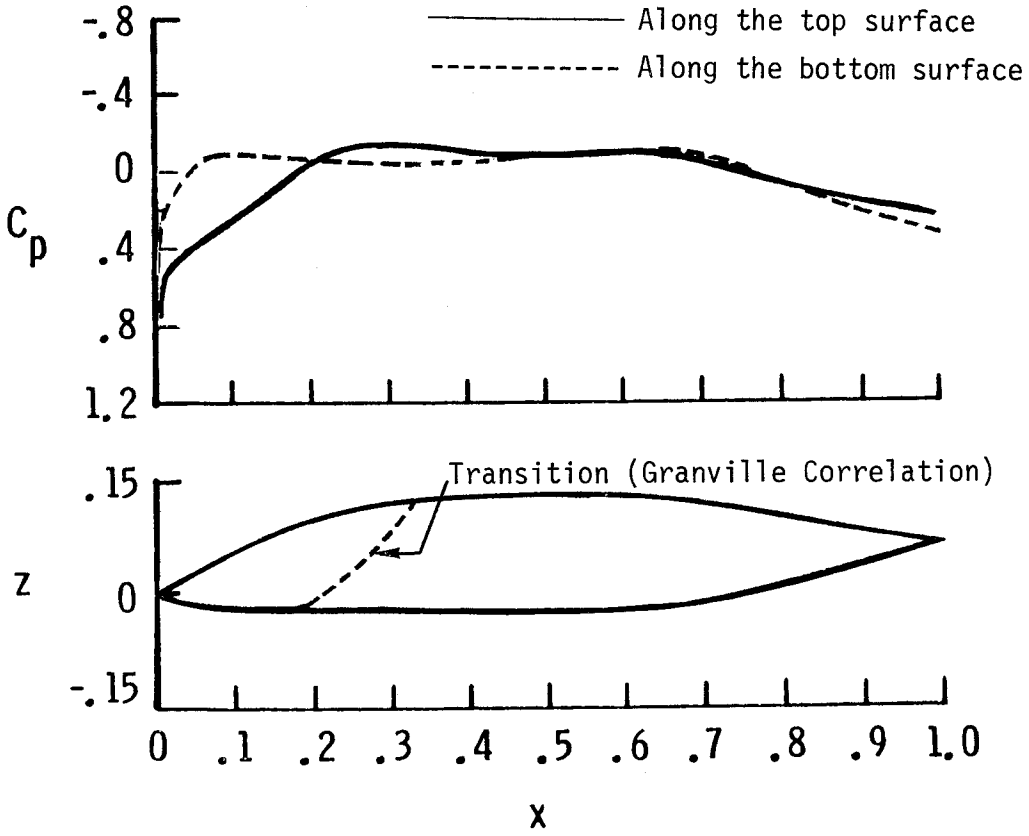


Figure 11. Surface Pressure Distribution, Geometry and Transition Location on a Representative Business Aircraft Fuselage; $\alpha = 0°$, $R_L$ = 40.86 million and Incompressible Flow.

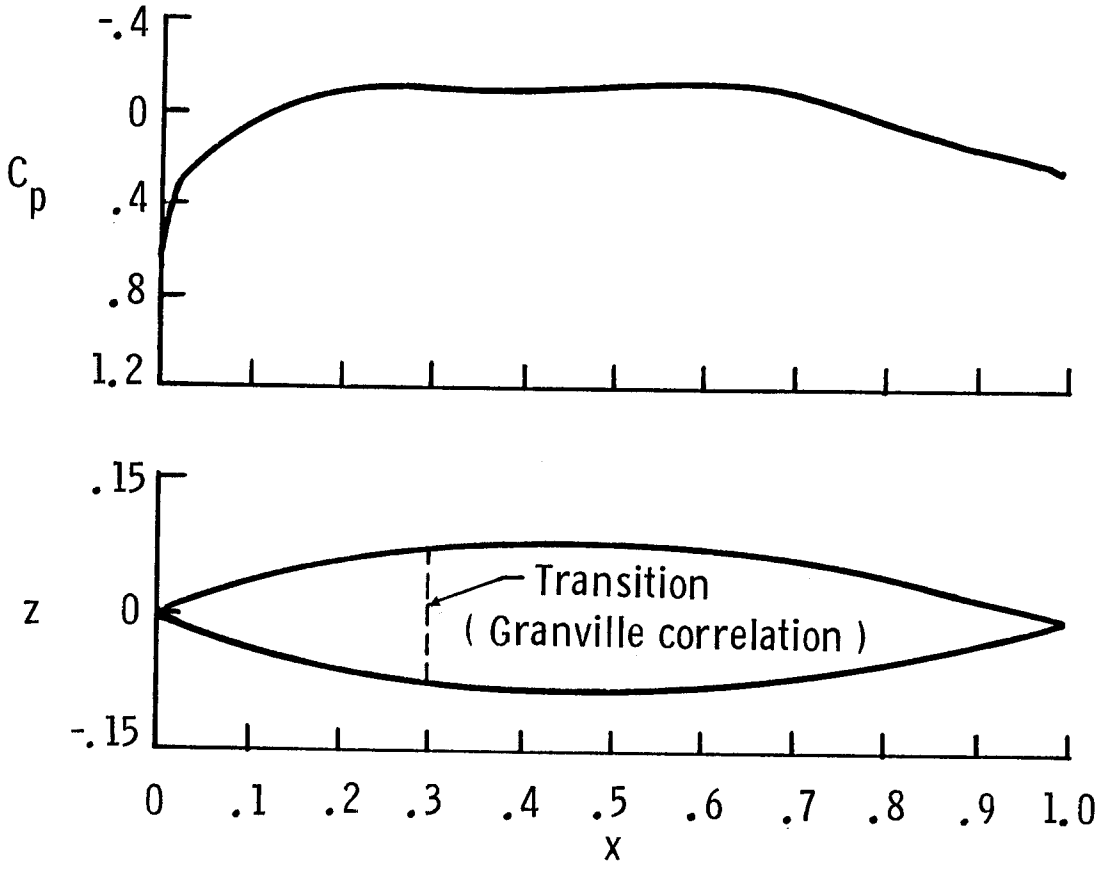


Figure 12. Surface Pressure Distribution, Geometry and Transition Location for a Body of Revolution in the Fineness Ratio 6.14; $\alpha = 0°$, $R_L = 40.86$ million and Incompressible Flow.

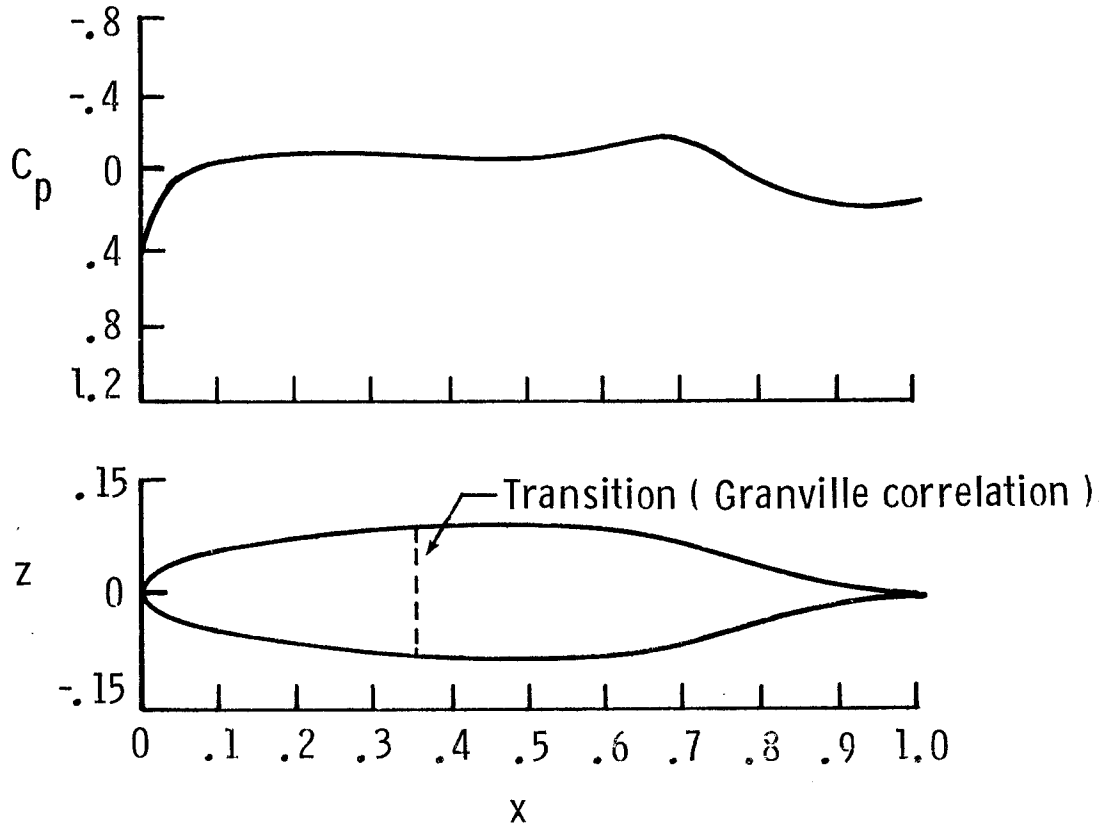


Figure 13. Surface Pressure Distribution, Geometry and Transition Location for Initial Body of Revolution, Fineness Ratio 6.14 and $R_L$ = 40.86 million and Incompressible Flow.

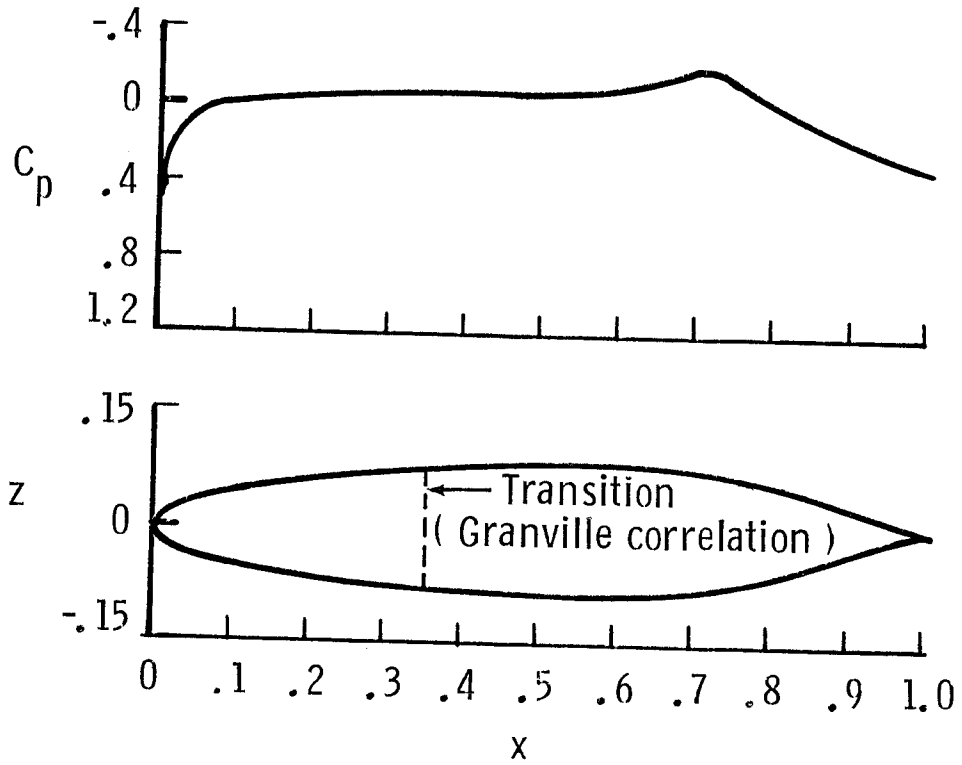


Figure 14. Surface Pressure Distribution, Geometry and Transition Location for Optimum Body of Revolution, Fineness Ratio 6.14, $R_L$ = 40.86 million and Incompressible Flow.

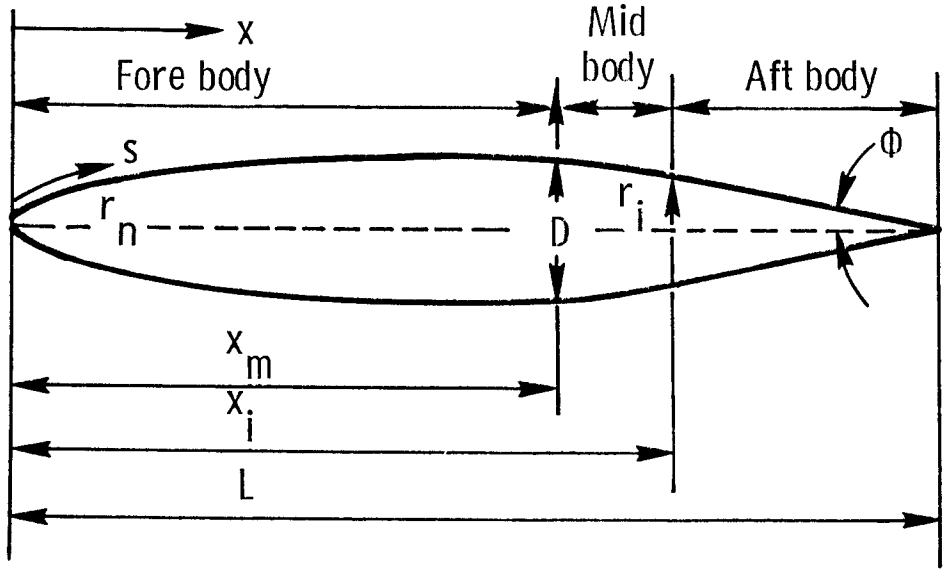


Figure 15. Definition of Parameters in the Optimization Procedure.